Trans. Tianjin Univ. (2017) 23:380–393
DOI 10.1007/s12209-017-0057-y

RESEARCH ARTICLE

Multi-objective Optimization of Non-uniform Beam for Minimum Weight and Sound Radiation

Furui Xiong[1,2] · Mengxin He[2] · Yousef Naranjani[3] · Qian Ding[2] · Jianqiao Sun[2,3]

Received: 29 April 2016 / Revised: 2 July 2016 / Accepted: 22 July 2016 / Published online: 19 May 2017

Abstract A multi-objective optimization of non-uniform beams is presented for minimum radiated sound power and weight. The transfer matrix method is used to compute the structural and acoustic responses of a non-uniform beam accurately and efficiently. The multi-objective particle swarm optimization technique is applied to search the Pareto optimal solutions that represent various compromises between weight and sound radiation. Several constraints are imposed, which substantially reduce the volume fraction of feasible solutions in the design space. Two non-uniform beams with different boundary conditions are studied to demonstrate the multi-objective optimal designs of the structure.

Keywords Non-uniform beams · Sound radiation · Transfer matrix method · Multi-objective optimization · Particle swarm technique

Introduction

Engineering structures are often designed and optimized to meet multiple and possibly conflicting objectives such as minimum weight and maximum strength. The merit of multi-objective optimization is to obtain a wide range of structural design choices so that the best tradeoff among different objectives can be achieved. This paper presents a multi-objective structural–acoustic optimization study of engineering structures. Specifically, we take non-uniform beams as an example.

A non-uniform beam is a common structural element in many applications. Many studies have been conducted on vibration, stability, and fatigue of non-uniform beams [1–3]. Numerous methods for solving vibration problems have also been studied, such as the finite element method [4], transfer matrix [5], and differential transfer [6]. Optimization of structural–acoustic properties is an important study of non-uniform beams. Adali studied the Pareto optimization of beams with a moving boundary in the 1980s [7]. Eschenauer et al. applied both deterministic and stochastic optimization for weight and static deflection reduction of non-uniform beams [8]. Continuous non-uniform beam optimization was considered in [9]. Optimization of boundary conditions was studied in [10]. Vibro-acoustic optimization was studied in [4, 11].

Two general categories of algorithms for solving multi-objective optimization problems (MOPs) exist. One is deterministic, and the other is evolutionary; the latter dominates among these categories. Representative deterministic search algorithms include multi-objective steepest descent [12], direct search [13], tangent space continuation [14], set-oriented algorithms [15], and cell mapping [16]. The convergence and global coverage of the Pareto set by deterministic algorithms can be usually guaranteed [12, 17]. However, for high-dimensional MOPs, deterministic algorithms face the curse of dimensionality. In addition, deterministic algorithms also have the drawback of being trapped in the local minima.

✉ Furui Xiong
xfr90311@gmail.com

[1] Science and Technology on Reactor System Design Technology Laboratory, Nuclear Power Institute of China, Chengdu 610041, China

[2] School of Mechanical Engineering, Tianjin University, Tianjin 300072, China

[3] School of Engineering, University of California Merced, Merced, CA 95343, USA

Evolutionary algorithms are stochastic and obtain the Pareto set in the form of a collection of random points in the design space. Therefore, evolutionary algorithms are not limited by the dimension of the problem. The mainstream evolutionary algorithms for MOPs include genetic algorithms [18, 19], multi-objective particle swarm optimization (MOPSO) [20], and the strength Pareto evolutionary algorithm [21]. This paper aims to solve the MOP of non-uniform beams with a modified particle swarm optimization (PSO) technique.

Multi-objective Particle Swarm Optimization

An MOP usually involves more than one conflicting objective. Unlike single-objective optimization problems, the solution of MOP usually forms a set. The definition of Pareto optimality is based on the concept of dominance.

Consider an MOP as

$$\min_{\boldsymbol{k}\in Q}\{\boldsymbol{F}(\boldsymbol{k})\}, \tag{1}$$

where $\boldsymbol{k} \in Q \subset \mathbf{R}^q$ is a q-dimensional vector of design parameters; $\boldsymbol{F}$ is the map that consists of the objective function $f_i \,:\, Q \to \mathbf{R}^1$.

$$\boldsymbol{F} \,:\, Q \to \mathbf{R}^m,\ \ \boldsymbol{F}(\boldsymbol{k}) = [f_1(\boldsymbol{k}), \ldots, f_m(\boldsymbol{k})]. \tag{2}$$

The design space $Q \subset \mathbf{R}^q$ can be expressed in terms of inequality and equality constraints

$$\begin{aligned} Q := \{\boldsymbol{k} \in \mathbf{R}^q \mid g_j(\boldsymbol{k}) \le 0,\ j = 1, \ldots, l,\\ \text{and } g_j(\boldsymbol{k}) = 0,\ j = l+1, \ldots, m\}. \end{aligned} \tag{3}$$

(a) Let $\boldsymbol{v}, \boldsymbol{w} \in \mathbf{R}^m$. The vector $\boldsymbol{v}$ is said to be less than or equal to $\boldsymbol{w}$ denoted as $\boldsymbol{v} \le_p \boldsymbol{w}$ if $v_i \le w_i$ for all $i \in \{1, \ldots, m\}$.

(b) A vector $\boldsymbol{v} \in Q$ is said to be dominated by a vector $\boldsymbol{w} \in Q$ denoted as $\boldsymbol{w} \prec \boldsymbol{v}$ with respect to MOP (1) if $\boldsymbol{F}(\boldsymbol{w}) \le_p \boldsymbol{F}(\boldsymbol{v})$ and $\boldsymbol{F}(\boldsymbol{w}) \ne \boldsymbol{F}(\boldsymbol{v})$. Otherwise, $\boldsymbol{v}$ is non-dominated by $\boldsymbol{w}$.

(c) A point $\boldsymbol{w} \in Q$ is called Pareto optimal or a Pareto point of MOP (1) if no $\boldsymbol{v} \in Q$ dominates $\boldsymbol{w}$.

(d) The set $\boldsymbol{P}$ of all Pareto optimal solutions is called the Pareto set. The image $\boldsymbol{F}(\boldsymbol{P})$ of $\boldsymbol{P}$ is called the Pareto front.

MOPSO integrates the non-dominant sorting and adaptive meshing in the objective space to reach the convergence and spreading of an evolutionary algorithm [20, 22]. The basic procedure of MOPSO is similar to that of the traditional single-objective PSO where the movements of each particle are influenced by the local best position and the current global best position [23].

The velocity v_i^m of particle i in the mth generation is updated to v_i^{m+1} in the next generation according to the following equation:

$$v_i^{m+1} = \omega\, v_i^m + R_1(B_i - p_i) + R_2(A_h - p_i), \tag{4}$$

where p_i is the current position of particle i in the design space; B_i is the best position occupied by particle i; ω is the inertia factor; R_1 and R_2 are two uniformly distributed random numbers in $[0, 1]$; and A_h is the reference particle of the current generation selected according to the measurement of particle distribution in the objective space. In this study, we set $\omega = 0.4$ as suggested in [24]. Equation (4) has the same form as that of the single-objective PSO. However, the local and global best positions are determined by non-dominant relationships.

Table 1 presents the procedure of MOPSO. An archive denoted as A is created to store non-dominant particles generated at each iteration. The archive is updated constantly to ensure its non-dominancy. As will be shown in the following section, feasible points occupy only a small portion of the volume of the design space.

Before Eq. (4) is applied, a fitness function is evaluated to determine A_h. The procedure is listed in Table 2. The objective space is discretized into a collection of cells, and the number of points that fall in each cell is counted. A fitness value is assigned, and cells that contain more particles are penalized. In other words, a greater number of particles in one cell correspond to a lower fitness value assigned to that cell to maintain an even level of particle spreading. The normalized fitness value serves as the selection probability of a cell from the roulette wheel run. Let z denote the cell chosen from the roulette wheel selection. A_h is determined by selecting a random particle from cell z.

The dominance check is applied to update the archive when a new position of one particle is calculated. Let p_i denote the new position of particle i at a certain generation. The principle to update the archive is to keep all non-empty positions being occupied with non-dominant points in the archive. Therefore, if p_i dominates $A_j \in A$, then A_j will be removed. On the other hand, if p_i is dominated by any element in the archive A, then p_i will not be added to the archive. Hence, the current position of particle i is not a potential solution.

Note that the capacity of the archive is usually larger than the population size but is still finite. During the evolution, the archive might be full. Under this circumstance, a secondary criterion will be applied to determine whether to add the new particle position to the archive. The code to enforce this criterion is presented in Table 3.

To avoid the population from being trapped in the local optimum, the mutation operator is introduced. The percentage of the mutated population decays exponentially with respect to the number of the current generation [20],

Table 1 Main structure of the MOPSO algorithm

Program: MOPSO

Input arguments: Searching boundary lb, ub, MOP $\boldsymbol{F}$, archive capability $A_{\max}$,
population size $p_{\max}$, number of generations $g_{\max}$,
objective space partition N_P, mutation rate r

Output argument: Non-dominant population p

Initialization by generating $p_{\max}$ feasible points and store in p.
Assign archive $A \leftarrow p$ and best current position array $B \leftarrow p$
for $gen = 1, g_{\max}$
    $A_h \leftarrow$ fitness(A, N_P)
    for $i = 1, p_{\max}$
        $v_i \leftarrow \omega v_i + R_1(B_i - p_i) + R_2(A_h - p_i)$
        $p_i \leftarrow p_i + v_i$
        if any element of the coordinate vector of p_i is out of the boundary,
            assign a boundary value and the negative velocity of that element
        end if
        if p_i violates constraints, **continue**
        $ndom \leftarrow$ **true**
        for $j = 1$, size(A)
            if $p_i \prec A_j$, remove A_j from archive
            elseif $A_j \prec p_i$, $ndom \leftarrow$ **false, break**
        end for
        if *ndom* **AND** archive is not full
            insert p_i into A
        elseif *ndom* **AND** archive is full
            $A \leftarrow$ adaptive_grid(A, p_i, N_P). Please refer to Table 3.
        end if
        if $p_i \prec B_i$, $B_i \leftarrow p_i$; **elseif** $p_i \nprec B_i$, B_i is randomly assigned by B_i or p_i
    end for
    $p \leftarrow$ mutation($p, gen, g_{\max}, p_{\max}, r, lb, ub$)
end for. Perform dominance check over A.

Table 2 Pseudo code of fitness assignment in the objective space

Program: Fitness

Input arguments: Current archive A, objective space partition N_P

Output argument: Best global individual A_h

1: Divide objective space of A into cells with the partition N_P

2: $S \leftarrow$ Cell set with at least one point dropping in it

3: Assign fitness value of each cell in S as $\frac{10}{\text{Number of points in each cell}}$

4: $S_h \leftarrow$ Roulette wheel selection from S according to fitness value

5: $A_h \leftarrow$ Randomly selected point within cell S_h

Table 3 Pseudo code of archive update when the archive is full

Program: Archive update

Input arguments: Current archive A, individual p_i, objective space partition N_P

Output argument: Updated archive A

1: Divide objective space of $A \cup p_i$ with partition N_P

2: $S_{\max}, S_{\min} \leftarrow$ cell with maximum/minimum number of points dropping in it

3: **if** p_i is within cell $S_{\min}$

4: Delete one randomly selected point in cell $S_{\max}$ from A

5: Insert p_i into A

6: **end if**

$$p_r = \exp\left(-\frac{15gen}{g_{\max}}\right), \tag{5}$$

where p_r is the percentage of population being mutated; gen is the current number of generations; and $g_{\max}$ is the maximum number of generations. The mutation occurs only in the first few generations where the landscape of the potential solutions is unknown. The pseudo code of the mutation operator is shown in Table 4.

Structural–Acoustic Analysis

Before we formulate a multi-objective structural–acoustic optimization problem, we present the structural–acoustic analysis of non-uniform beams by applying the transfer matrix method [5].

Vibration Analysis

We use a Euler–Bernoulli beam to demonstrate the multi-objective structural–acoustic optimization problem in this study. The equation of motion is given by

$$D(x)\frac{\partial^4 w}{\partial x^4} + c(x)\frac{\partial w}{\partial t} + \gamma(x)\frac{\partial^2 w}{\partial t^2} = g(x, t),\ 0 \le x \le L, \tag{6}$$

where $D(x)$ is the beam rigidity; $\gamma(x)$ is the mass per unit area; $c(x)$ is the structural damping; $g(x, t)$ is the external excitation; and $w(x, t)$ is the deflection of the beam. We consider the Rayleigh damping here, namely $c(x) = \alpha\gamma(x) + \eta D(x)$. Furthermore, we assume that $D(x)$, $\gamma(x)$, and $c(x)$ are given smooth functions of x.

The transfer matrix method proposes to divide the beam into N uniform segments such that $D(x)$ and $\gamma(x)$ can be written as

Table 4 Pseudo code of the mutation process

Program: Mutation

Input arguments: Current generation gen, maximum generation $g_{\max}$, current population p, population size $p_{\max}$, mutation rate r, searching boundary lb, ub

Output argument: Mutated population p

```
1: p_r ← exp(−15gen/g_max), which is the mutation percentage over the entire population
2: M_n ← round(p_r p_max), which is the number of particles being mutated
3: if M_n ≠ 0
4:     S ← subset of M_n randomly selected particles from p
5:     for i = 1, M_n
6:         x ← (1 − gen/g_max)^(5/r)
7:         if x > 10^−4
8:             j ← randomly selected number from 1 to search space dimension
9:             Δ ← x[ub(j) − lb(j)]
10:            S_i(j) ← random number within the range of [S_i(j) − Δ, S_i(j) + Δ]
11:        end if
12:    end for
13:    Replace the old subset of p with the new S
14: end if
```

$$D(x)=\begin{cases}D_1, & \beta_1\le x\le\beta_2\\ \vdots & \\ D_i, & \beta_i\le x\le\beta_{i+1}\\ \vdots & \\ D_N, & \beta_N\le x\le\beta_{N+1}\end{cases},\qquad \gamma(x)=\begin{cases}\gamma_1, & \beta_1\le x\le\beta_2\\ \vdots & \\ \gamma_i, & \beta_i\le x\le\beta_{i+1}\\ \vdots & \\ \gamma_N, & \beta_N\le x\le\beta_{N+1}\end{cases}, \tag{7}$$

where β_i and β_{i+1} are the coordinates of both ends of the ith segment, and $\beta_1=0$ and $\beta_{N+1}=L$. The free undamped vibration of each segment satisfies the following equation:

$$D_i\frac{\partial^4 w}{\partial x^4}+\gamma_i\frac{\partial^2 w}{\partial t^2}=0,\ \ \beta_i\le x\le\beta_{i+1}. \tag{8}$$

Consider the harmonic response of the ith segment as $w(x,t)=X_i(x)\,\mathrm{e}^{\mathrm{j}\omega t}$. We have

$$D_iX_i''''-\gamma_i\omega^2X_i=0,\ \ \beta_i\le x\le\beta_{i+1}. \tag{9}$$

The general solution of Eq. (9) is given by

$$X_i(x)=X_i(\beta_i)f_1(\varphi_i)+\frac{X_i'(\beta_i)}{k_i}f_2(\varphi_i)+\frac{M_i(\beta_i)}{D_ik_i^2}f_3(\varphi_i)+\frac{Q_i(\beta_i)}{D_ik_i^3}f_4(\varphi_i)\,, \tag{10}$$

where $k_i^4=\frac{\gamma_i\omega^2}{D_i}$, $\varphi_i=k_i(x-\beta_i)$ and

$$M_i(x)=D_i\frac{\partial^2X_i}{\partial x^2},\ \ Q_i(x)=D_i\frac{\partial^3X_i}{\partial x^3}, \tag{11}$$

and

$$f_1(\varphi_i) = \tfrac{1}{2}[\cosh(\varphi_i) + \cos(\varphi_i)], \quad f_2(\varphi_i) = \tfrac{1}{2}[\sinh(\varphi_i) + \sin(\varphi_i)],$$
$$f_3(\varphi_i) = \tfrac{1}{2}[\cosh(\varphi_i) - \cos(\varphi_i)], \quad f_4(\varphi_i) = \tfrac{1}{2}[\sinh(\varphi_i) - \sin(\varphi_i)]. \tag{12}$$

The functions in Eq. (12) satisfy the following relations:

$$\frac{\partial f_1}{\partial x} = k_i f_4, \quad \frac{\partial f_2}{\partial x} = k_i f_1, \quad \frac{\partial f_3}{\partial x} = k_i f_2, \quad \frac{\partial f_4}{\partial x} = k_i f_3. \tag{13}$$

Define a vector $\boldsymbol{u}_i = \left[X_i(\beta_i),\, X_i'(\beta_i),\, M_i(\beta_i),\, Q_i(\beta_i)\right]^{\mathrm{T}}$. From Eqs. (10) and (11), we can evaluate $\boldsymbol{u}_{i+1} = \left[X_i(\beta_{i+1}),\, X_i'(\beta_{i+1}),\, M_i(\beta_{i+1}),\, Q_i(\beta_{i+1})\right]^{\mathrm{T}}$, leading to the following transfer relationship:

$$\boldsymbol{u}_{i+1} = \boldsymbol{A}_i \boldsymbol{u}_i, \tag{14}$$

$$\boldsymbol{A}_i = \begin{bmatrix} f_1 & \frac{f_2}{k_i} & \frac{f_3}{D_i k_i^2} & \frac{f_4}{D_i k_i^3} \\ k_i f_4 & f_1 & \frac{f_2}{D_i k_i} & \frac{f_3}{D_i k_i^2} \\ D_i k_i^2 f_3 & D_i k_i f_4 & f_1 & \frac{f_1}{k_i} \\ D_i k_i^3 f_2 & D_i k_i^2 f_3 & k_i f_4 & f_1 \end{bmatrix}_{x=\beta_{i+1}}, \tag{15}$$

where $\boldsymbol{A}_i$ is known as the transfer matrix of one segment. By repeating this process over all segments, we obtain the transfer relationship from $\boldsymbol{u}_1$ to $\boldsymbol{u}_{N+1}$ as

$$\boldsymbol{u}_{N+1} = \boldsymbol{A}_N \boldsymbol{A}_{N-1} \cdots \boldsymbol{A}_2 \boldsymbol{A}_1 \boldsymbol{u}_1 \equiv \boldsymbol{B}\boldsymbol{u}_1, \tag{16}$$

where the matrix $\boldsymbol{B}$ is the transfer matrix of the beam from $x = 0$ to $x = L$. Note that $\boldsymbol{B}$ is a function of the frequency ω and that $\boldsymbol{u}_1$ and $\boldsymbol{u}_{N+1}$ must satisfy the boundary conditions.

After imposing the boundary conditions to $\boldsymbol{u}_1$ and $\boldsymbol{u}_{N+1}$ in Eq. (16), we obtain the transcendental equation for determining the natural frequencies of the beam. Examples of transcendental equations for different boundary conditions are shown in Table 5.

Let ω_n be the nth natural frequency of the beam obtained from the transcendental equation and $X_{ni}(x)$ be the corresponding mode function of the ith segment. The nth mode function of the beam can be written as

$$\varphi_n(x) = \begin{cases} X_{n1}(x), & \beta_1 \le x \le \beta_2 \\ \vdots & \\ X_{ni}(x), & \beta_i \le x \le \beta_{i+1} \\ \vdots & \\ X_{nN}(x), & \beta_N \le x \le \beta_{N+1} \end{cases} \tag{17}$$

We assume that $\varphi_n(x)$ is normalized such that

$$\int_0^L \gamma(x)\, \varphi_n^2(x)\, \mathrm{d}x = \sum_{i=1}^{N} \gamma_i \int_{\beta_i}^{\beta_{i+1}} X_{ni}^2(x)\, \mathrm{d}x = 1. \tag{18}$$

The mode functions are orthogonal,

$$\int_0^L \gamma(x) \varphi_m(x) \varphi_n(x) \mathrm{d}x = \sum_{i=1}^{N} \gamma_i \int_{\beta_i}^{\beta_{i+1}} X_{mi}(x) X_{ni}(x) \mathrm{d}x = \delta_{mn}, \tag{19}$$

$$\int_0^L D(x)\, \varphi_m''''(x)\, \varphi_n(x)\, \mathrm{d}x = \sum_{i=1}^{N} D_i \int_{\beta_i}^{\beta_{i+1}} X_{mi}''''(x) X_{ni}(x) \mathrm{d}x = \omega_n^2 \delta_{mn}. \tag{20}$$

Consider a harmonic external excitation $g(x, t) = G(x)\, \mathrm{e}^{\mathrm{j}\omega t}$ and a complex harmonic response of the beam $w(x, t) = X(x)\, \mathrm{e}^{\mathrm{j}\omega t}$ such that the spatial part of the function can be expanded in terms of the mode functions

$$X(x) = \sum_{n=1}^{\infty} W_n\, \varphi_n(x), \quad G(x) = \sum_{n=1}^{\infty} G_n\, \gamma(x)\, \varphi_n(x), \tag{21}$$

where W_n is the modal expansion coefficient of the response, and G_n can be computed as

$$G_n = \int_0^L \gamma(x)\, G(x)\, \varphi_n(x) \mathrm{d}x. \tag{22}$$

From Eq. (6) together with the orthogonality properties of the mode functions, we obtain

$$W_n = \frac{G_n}{\omega_n^2 - \omega^2 + \mathrm{j}\omega\,(\alpha + \eta\omega_n^2)}. \tag{23}$$

The forced damped solution of Eq. (6) then reads

$$w(x, t) = \sum_{n=1}^{\infty} W_n\, \varphi_n(x)\, \mathrm{e}^{\mathrm{j}\omega t} = \sum_{n=1}^{\infty} \frac{G_n \cdot \varphi_n(x)}{\omega_n^2 - \omega^2 + \mathrm{j}\omega\,(\alpha + \eta\omega_n^2)} \mathrm{e}^{\mathrm{j}\omega t}. \tag{24}$$

Acoustic Analysis

The wavenumber transformation of a mode function is defined as [5]

$$\Phi_n(k) = \int_{-\infty}^{\infty} \varphi_n(x)\, \mathrm{e}^{\mathrm{j}kx} \mathrm{d}x = \int_0^L \varphi_n(x)\, \mathrm{e}^{\mathrm{j}kx} \mathrm{d}x = \sum_{i=1}^{N} \int_{\beta_i}^{\beta_{i+1}} X_{ni}(x)\, \mathrm{e}^{\mathrm{j}kx} \mathrm{d}x. \tag{25}$$

Table 5 Transcendental equations for different boundary conditions of the non-uniform beam

Boundary condition	Component form	Transcendental equation
Simply supported	$X(0) = M(0) = X(L) = M(L) = 0$	$\boldsymbol{B}_{12}\boldsymbol{B}_{34} - \boldsymbol{B}_{32}\boldsymbol{B}_{14} = 0$
Clamped–clamped	$X(0) = X'(0) = X(L) = X'(L) = 0$	$\boldsymbol{B}_{13}\boldsymbol{B}_{24} - \boldsymbol{B}_{23}\boldsymbol{B}_{14} = 0$
Cantilever	$X(0) = X'(0) = M(L) = Q(L) = 0$	$\boldsymbol{B}_{33}\boldsymbol{B}_{44} - \boldsymbol{B}_{34}\boldsymbol{B}_{43} = 0$

The wavenumber transformation of the deflection velocity of the forced response of the beam is an interesting function that reveals the acoustic property [5].

The spatial distribution of the deflection velocity of the forced response of the beam can be derived from the closed-form solution in Eq. (24),

$$v(x) = \sum_{n=1}^{\infty} \mathrm{j}\omega\, W_n\, \varphi_n(x). \tag{26}$$

The wavenumber transformation of the velocity is given by

$$\begin{aligned} V(k) &= \int_{-\infty}^{\infty} v(x)\, \mathrm{e}^{\mathrm{j}kx} \mathrm{d}x = \int_0^L v(x)\, \mathrm{e}^{\mathrm{j}kx} \mathrm{d}x \\ &= \sum_{n=1}^{\infty} \mathrm{j}\omega\, W_n\, \Phi_n(k). \end{aligned} \tag{27}$$

The average acoustic power radiated by the vibrating beam per unit width over one period of vibrations can be computed as [5]

$$\bar{P} = \frac{\omega \rho_0}{4\pi} \int_{-k}^{k} \frac{V(\hat{k})\, V^*(\hat{k})}{\sqrt{k^2 - \hat{k}^2}} \mathrm{d}\hat{k}, \tag{28}$$

where $k = \omega / c_0$ is the wavenumber of the air at the frequency ω; c_0 is the speed of sound; and ρ_0 is the air density. $(\ )^*$ denotes the complex conjugate.

Let $\langle v^2 \rangle$ be the spatial and temporal average of the deflection velocity field of the beam given by

$$\langle v^2 \rangle = \frac{1}{L} \int_0^L v(x)\, v^*(x)\, \mathrm{d}x. \tag{29}$$

The radiation efficiency of the vibrating beam is defined as

$$\sigma = \frac{\bar{P}}{\frac{1}{2}\rho_0\, c_0 L \langle v^2 \rangle}. \tag{30}$$

Some computational notes are in order. The computations of Eqs. (28) and (30) require numerical integrations. The analytical expression of the integration in Eq. (25) helps speed up these numerical integrations. The transfer matrix method for structural–acoustic analysis offers a fast and accurate approach for multi-objective optimization studies.

Structural–Acoustic Optimization

Design Variables

The geometric and material properties of the non-uniform beam are assumed to be continuous functions of the spatial coordinate x. In the following discussions, we assume that only the thickness of the beam denoted as $h(x)$ is non-uniform. We take a number of the sampled thickness $h(x_i)$ along the beam as design variables and use them to construct the smooth function $h(x)$ by means of spline interpolation.

Figure 1 shows an example of a cubic spline representation of the thickness profile $h(x)$ with five sampled points. Figure 1b shows 10 sampled thicknesses, while Fig. 1c shows the 10-segment stepped beam based on the sampled thicknesses that are used with the transfer matrix method. The number of segments is a user-defined variable for the structural–acoustic analysis with the transfer matrix method. It affects the accuracy of the solution but does not increase the complexity of the optimization problem.

Objective Functions

The primary goal of structural–acoustic design is to create a lightweight and quiet structure. The multi-objective optimization of non-uniform beams aims to seek a balance between weight reduction and sound isolation.

The total mass of the beam can be expressed as

$$m_{\mathrm{tot}} = \sum_{i=1}^{N} \frac{\rho\, h_i\, L}{N}, \tag{31}$$

where ρ is the mass density of the beam; L is the length of the beam; h_i is the average thickness of the ith segment determined by the thickness profile; and N is the number of segments of the beam.

The second objective function is the integration of the radiated sound power in Eq. (28) over a range of frequencies

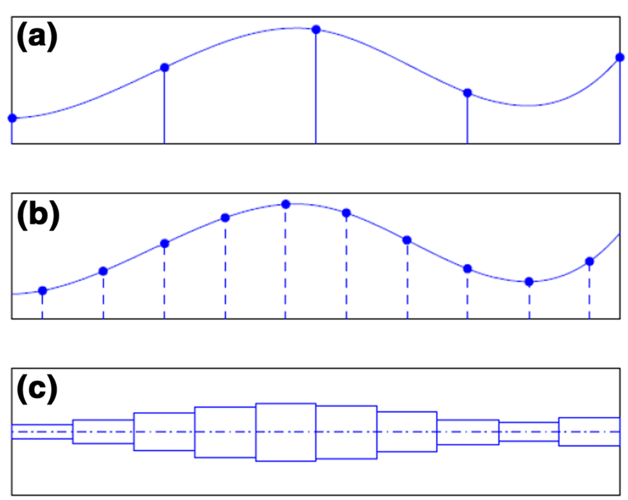

Fig. 1 Spline interpolation for the thickness profile $h(x)$ with the design variables $h(x_i)$. **a** the spline curve with five sampled points, **b** the spline curve with 10 sampled points, **c** the stepped beam of ten segments used in the solution with the transfer matrix method

Table 6 Parameters of the non-uniform beam

Young's modulus (Pa)	Mass density (kg/m^3)	Air density (kg/m^3)	Sound speed (m/s)	Beam width (m)
7×10^{10}	2643	1.26	343	0.1

Table 7 Statistical study of the volumetric fraction of feasible solutions in the design space

Number of sampled points in design space	1000	5000	10000	50000	100000	500000
Number of feasible points in five samplings	1	15	31	172	316	1522
	3	14	35	145	306	1528
	3	9	41	156	289	1512
	6	16	27	130	298	1499
	5	15	36	149	311	1518
Percent average of feasible points	0.36%	0.276%	0.34%	0.3008%	0.304%	0.3032%

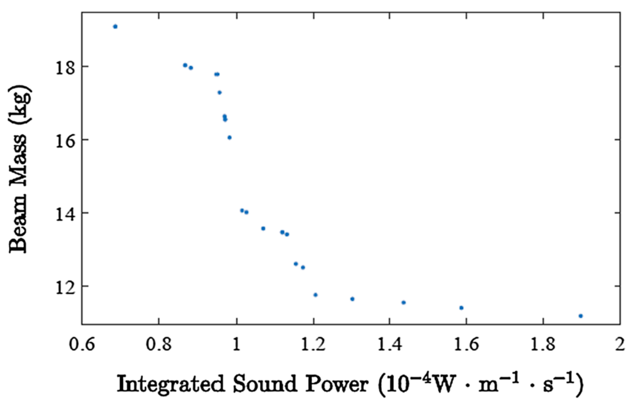

Fig. 2 Pareto front of the clamped–clamped beam. The population size of the MOPSO method is 100 with 80 generations. Twenty-one Pareto solutions are found

$$I = \int_{\omega_1}^{\omega_2} \bar{P}\,\mathrm{d}\omega, \tag{32}$$

where ω_1 and ω_2 define the lower and upper bounds of the frequencies of interest, respectively. These bounds are determined based on practical considerations in engineering applications. In this study, we assume that they are given.

Constraints

To ensure that the optimally designed structure meets engineering requirements, we impose three constraints for optimization.

1. The lower and upper bounds of the mass m_{tot}:

$$m_{\min} < m_{\mathrm{tot}} < m_{\max}. \tag{33}$$

2. The lower bound of the fundamental frequency ω_1.

$$\omega_{\min} < \omega_1. \tag{34}$$

This constraint guarantees minimum static strength for structural integrity.

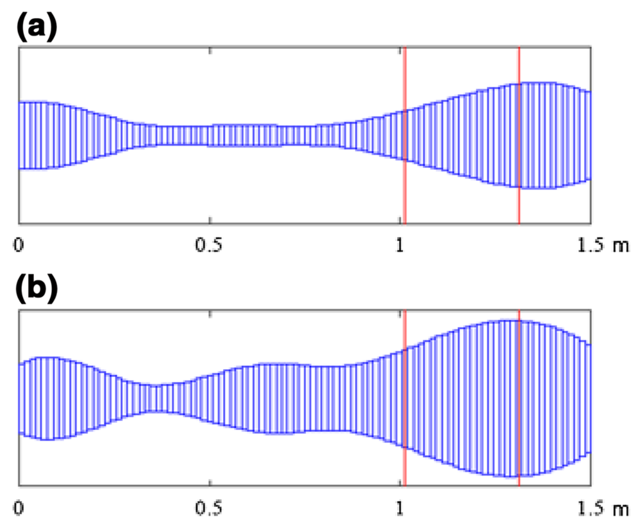

Fig. 3 Optimized thickness profile for the clamped–clamped beam. The harmonic load is applied in the interval marked by the red lines. **a** beam No. 1 has the minimum weight, while **b** beam No. 2 has the minimum integrated sound power

Table 8 Spline coordinates of the optimal clamped–clamped beam

x_i (m)	$h(x_i)$ of beam No. 1 (mm)	$h(x_i)$ of beam No. 2 (mm)
0	3.7282	3.7790
0.1667	2.9248	3.8781
0.3333	1.2039	1.5281
0.5000	1.1018	2.5685
0.6667	1.1118	3.9453
0.8333	1.2505	3.6051
1.0000	2.6231	5.2999
1.1667	4.5633	8.0084
1.3333	5.9476	8.7516
1.5000	4.7774	5.9250

3. The smoothness of the beam

$$\max_{i=1,\ldots,N} |h_{i+1} - h_i| < \Delta h. \tag{35}$$

Although the spline interpolation generates a smooth profile of the non-uniform beam, this constraint on the maximum height difference between two neighboring segments in the transfer matrix solution limits the sharp change in the thickness.

Numerical Results

Two case studies are presented in this section with different boundary conditions. For both cases, the number of interpolation coordinates, i.e., the number of design variables, is 10. The number of segments used by the transfer matrix method is 50. The material properties of the non-uniform beam are listed in Table 6. For all the optimization studies, we set the population size of the MOPSO method as 100, the

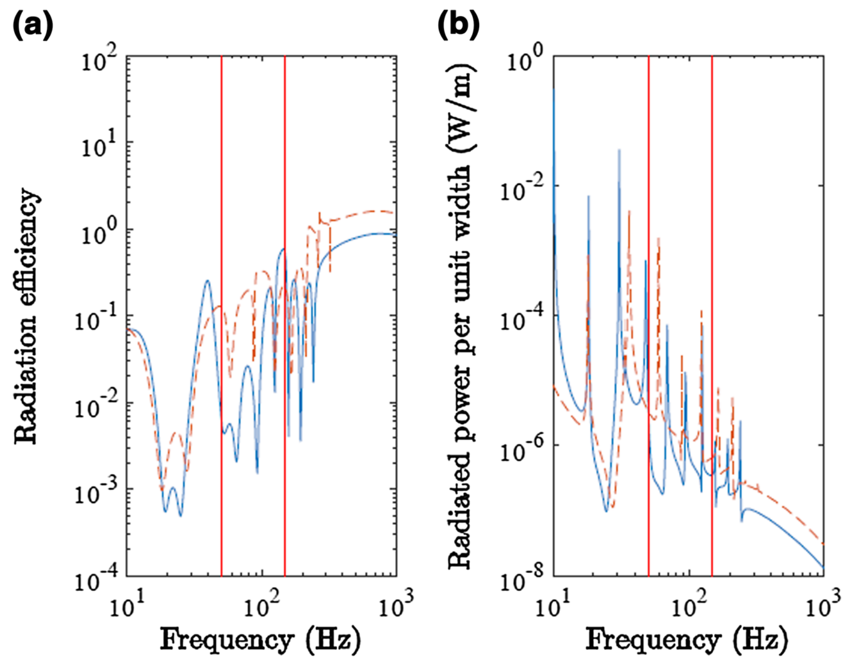

Fig. 4 **a** Sound radiation efficiency and **b** radiated sound power of beam No. 1 in Fig. 3. *Solid lines* the optimized non-uniform beam. *Dashed lines* the uniform beam with the same mass. The targeted frequency range is from 50 to 150 Hz

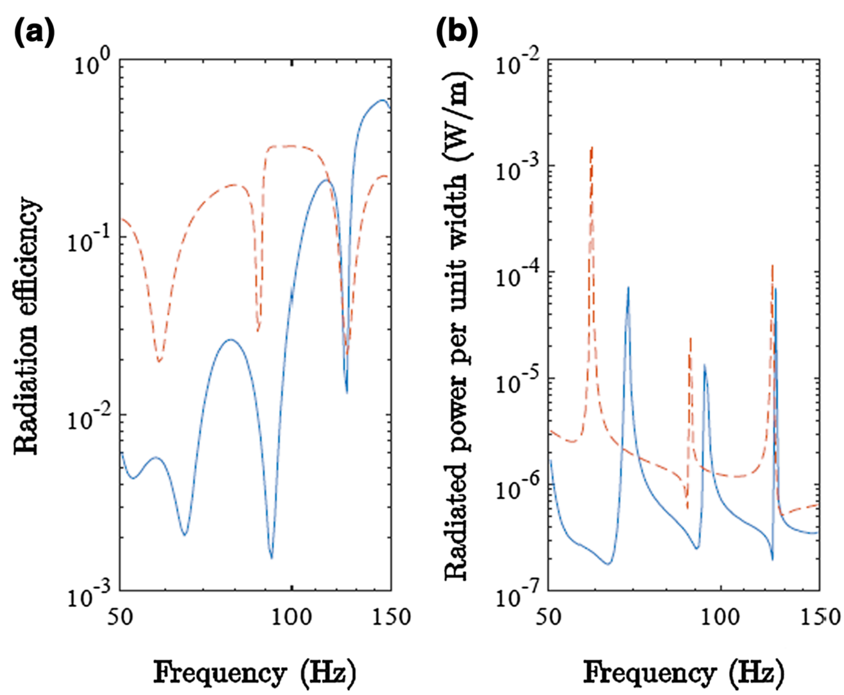

Fig. 5 Zoomed view of Fig. 4 in the frequency range 50–150 Hz. *Solid lines* the optimal non-uniform beam. *Dashed lines* the uniform beam with the same mass. Radiated sound power reduction of the optimal design is 68.99 dB compared with the baseline beam

number of generations as 80, and the archive size as 120. The mutation rate is 0.025. The MOPSO method is executed eight times for each scenario. The non-dominant solutions from all eight experiments are taken as the final result. The partition of the objective space for fitness value assignment is 30×30. All computations presented in this paper are conducted in a laptop with a 2.4 GHz i7-4700MQ CPU.

Clamped–Clamped Beam

The constraints defined in Eqs. (33)–(35) significantly reduce the feasible solutions in the design space. We discuss the feasible solutions in the design space first under the following constraints:

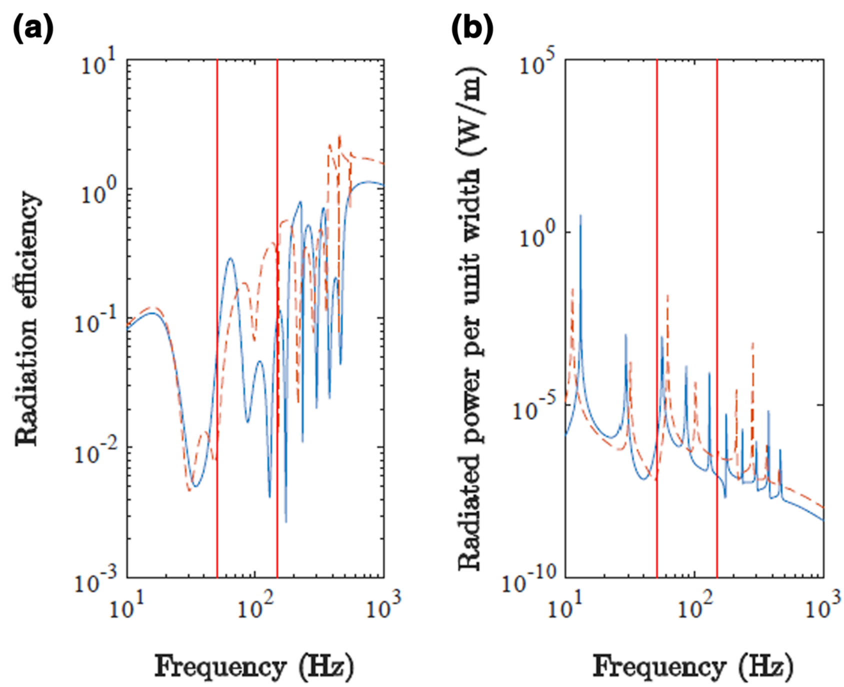

Fig. 6 **a** Sound radiation efficiency and **b** radiated sound power of beam No. 2 in Fig. 3. *Solid lines* the optimized non-uniform beam. *Dashed lines* the uniform beam with the same mass. The targeted frequency range is from 50 to 150 Hz

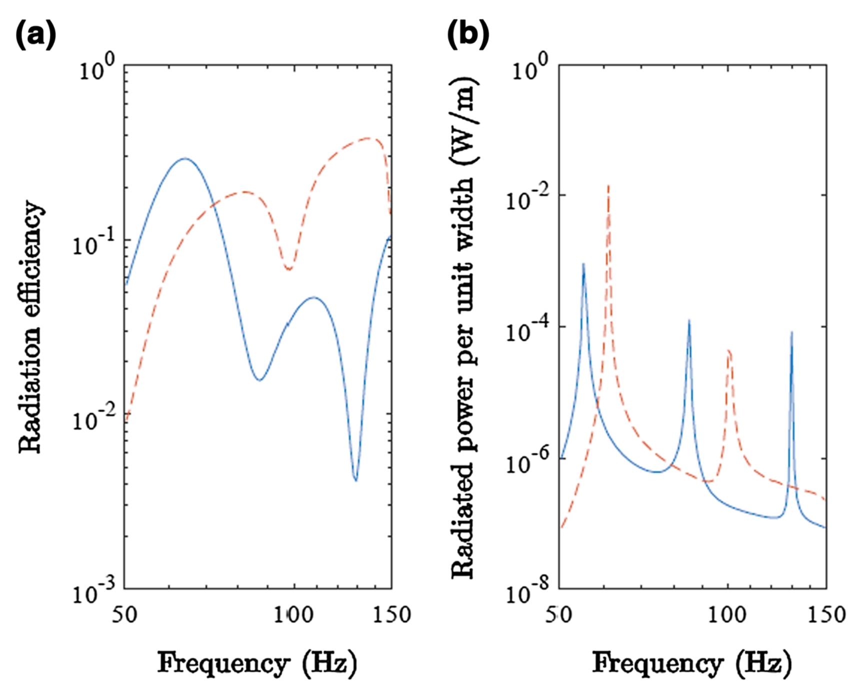

Fig. 7 Zoomed view of Fig. 6 in the frequency range 50–150 Hz. *Solid lines* the optimized non-uniform beam. *Dashed line* the uniform beam with the same mass. Radiated sound power reduction of the optimal design is 77.97 dB compared with the baseline beam

$$10\,\text{kg} < m_{\text{tot}} < 30\,\text{kg},\ \frac{\omega_1}{2\pi} > 10\,\text{Hz},$$
$$\max_{i=1,\dots,N} |h_{i+1} - h_i| < 1.75\,\text{mm}. \tag{36}$$

A uniform unit magnitude loading is applied to the beam in the interval $x \in [1.0125,\ 1.3125]$m. The frequency of the excitation sweep is in the range from 50 to 150 Hz. Hence, the excitation is equivalent to a bandlimited noise defined in this frequency range. This range represents the frequencies of interest. The bounds of the spline coordinates x_i are given by $1 \le x_i \le 10$ mm. The beam length is 1.5 m. The first 10 modes of the beam are used for the structural–acoustic analysis.

Table 7 presents the results of random samplings of feasible solutions in the design space for the clamped–clamped beam. The number of random sampling ranges from 1000 to half a million. We repeat the experiments five times to compute the average ratio of the feasible solutions. For this example, only 0.3% of the 10-dimensional design space is occupied by the feasible points. Therefore, the search for the Pareto set will be constrained within the 0.3% volume of the design space.

Figure 2 shows the Pareto front for the clamped–clamped beam, which consists of 21 solutions. The average computational time is 4765.2 s in the laptop. Figure 3 presents the thickness profile of two extreme designs, namely, the minimum weight and minimum sound radiation. The spline coordinates of the two extreme solutions are listed in Table 8. Figures 4 and 6 show the sound radiation efficiency and radiated sound power of the two beams. Both quantities are reduced in the frequency range [50, 150] Hz as compared with the baseline uniform beam of the same mass, as highlighted in Figs. 5 and 7. The average reduction of the radiated sound power over the frequency range is defined as

$$\Delta \bar{P} = 10\,\lg\left(\frac{\Delta \bar{P}_I}{P_0}\right)(\text{dB}), \tag{37}$$

$$\Delta \bar{P}_I = \frac{1}{\omega_2 - \omega_1}\int_{\omega_1}^{\omega_2} (\bar{P}_u - \bar{P}_n)\,\mathrm{d}\omega, \tag{38}$$

where $\bar{P}_u$ and $\bar{P}_n$ are the radiated sound power of the uniform and non-uniform beam, respectively; and $P_0 = 10^{-12}$ W is the sound power reference. The sound power reductions in the frequency range are 68.88 and 77.97 dB for the optimal designs shown in Figs. 5 and 7, respectively.

Simply Supported Beam

A uniform unit magnitude loading is applied to the beam in the interval $[0.4714,\ 0.7071]$m. The frequency sweeps in the range from 200 to 600 Hz. The bounds of the spline coordinates x_i are given by $1 \le x_i \le 15$ mm. The beam

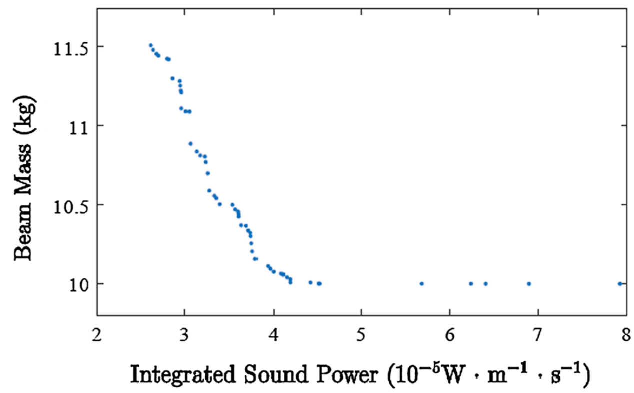

Fig. 8 Pareto front of the simply supported beam. The population size of the MOPSO method is 100 with 80 generations. Fifty-five Pareto solutions are found

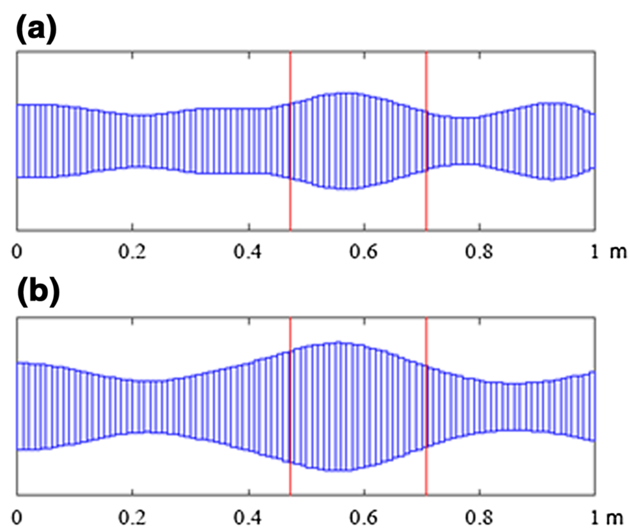

Fig. 9 Optimized thickness profile for the simply supported beam. The harmonic load is applied in the interval marked by the red lines. **a** beam No. 1 has the minimum mass, while **b** beam No. 2 has the minimum integrated sound power

Table 9 Spline coordinates of the optimal simply supported beam

x_i (m)	$h(x_i)$ of beam No. 1 (mm)	$h(x_i)$ of beam No. 2 (mm)
0	4.0342	4.8759
0.1111	3.6601	3.9679
0.2222	2.9467	2.8652
0.3333	3.6577	3.8399
0.4444	3.7620	5.7222
0.5556	5.3637	7.1958
0.6667	4.0507	5.4859
0.7778	2.5819	3.1875
0.8889	4.0279	2.6919
1.0000	2.7926	3.9287

length is 1.0 m. The first 10 modes of the beam are used for the structural–acoustic analysis. The lower bound of the minimum fundamental frequency is set as 8 Hz.

Figure 8 shows the Pareto front for the simply supported beam. Fifty-five solutions are found. The average computational time is 5042.7 s. Figure 9 presents the beam shape of two extreme designs. The corresponding spline coordinates are listed in Table 9. Figures 10 and 12 show the sound radiation efficiency and radiated sound power of the two beams. Both quantities are reduced in the frequency range [200, 600] Hz as compared with the baseline uniform beam of the same mass, as highlighted in Figs. 11 and 13 (Fig .12). The reductions of the radiated sound power are 35.13 and 39.19 dB in the frequency range of interest as shown in Figs. 11 and 13, respectively.

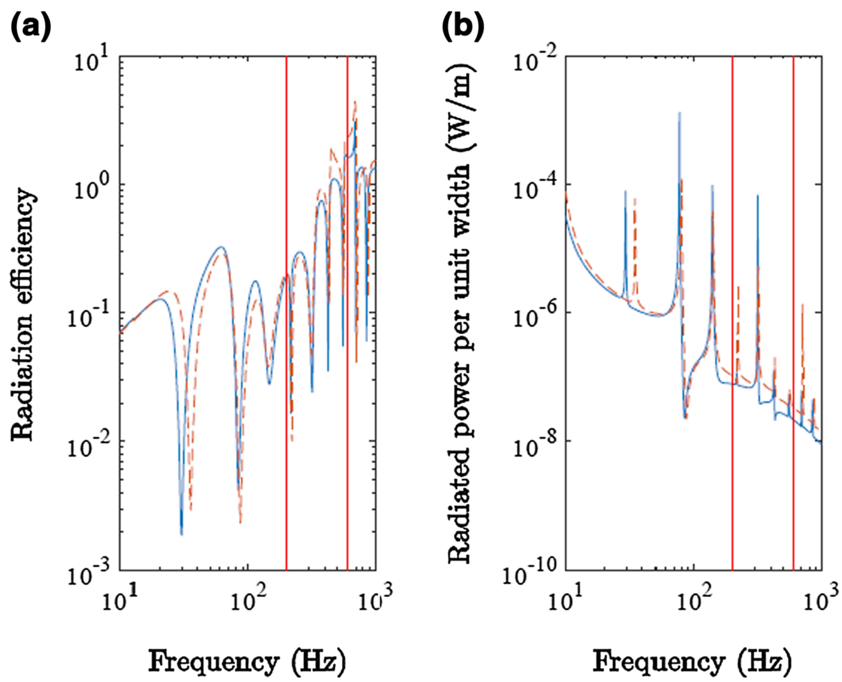

Fig. 10 **a** Sound radiation efficiency and **b** radiated sound power of beam No. 1 in Fig. 9. *Solid lines* the optimized non-uniform beam. *Dashed lines* the uniform beam with the same mass. The targeted frequency range is from 200 to 600 Hz

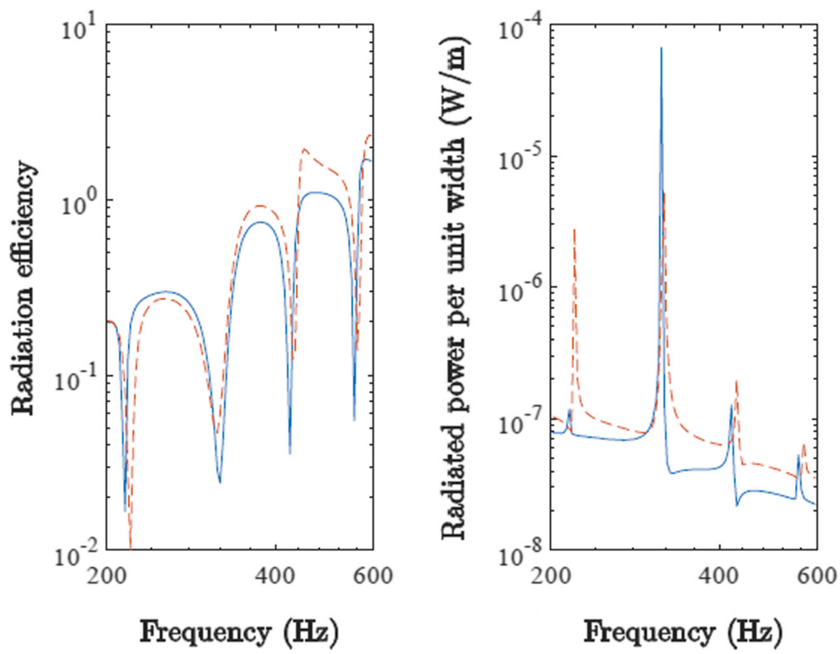

Fig. 11 Zoomed view of Fig. 10 in the frequency range 200–600 Hz. *Solid lines* the optimized non-uniform beam. *Dashed lines* the uniform beam with the same mass. Radiated sound power reduction of the optimal design is 35.13 dB compared with the baseline beam

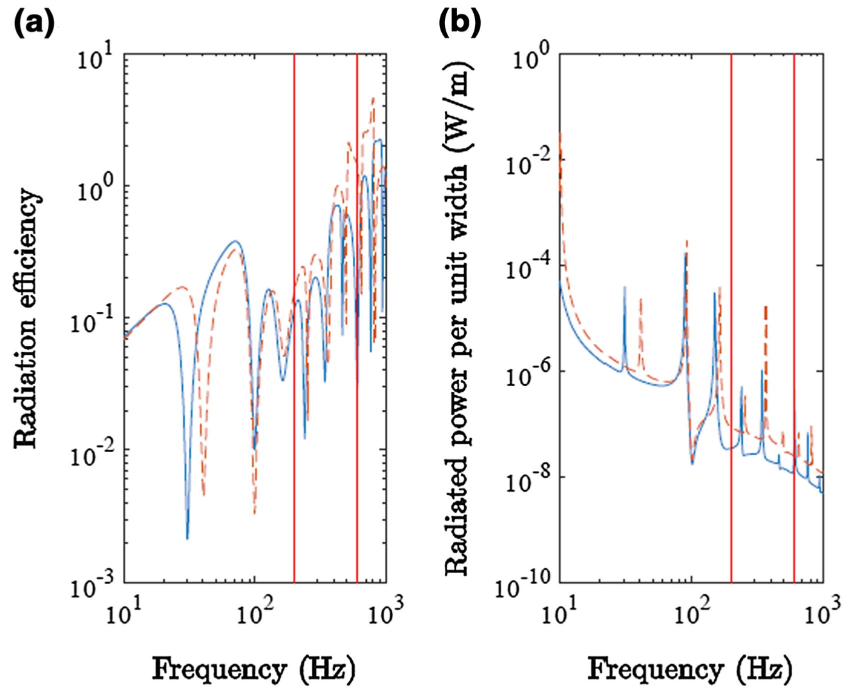

Fig. 12 **a** Sound radiation efficiency and **b** radiated sound power of beam No. 2 in Fig. 9. *Solid lines* the optimized non-uniform beam. *Dashed lines* the uniform beam with the same mass. The targeted frequency range is from 200 to 600 Hz

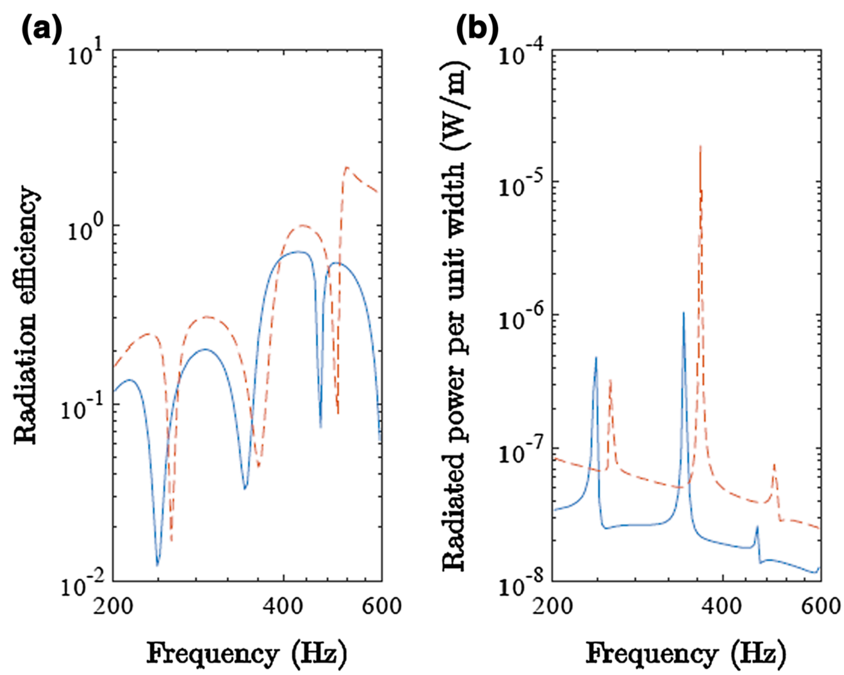

Fig. 13 Zoomed view of Fig. 12 in the frequency range 200–600 Hz. *Solid lines* the optimized non-uniform beam. *Dashed lines* the uniform beam with the same mass. The radiated sound power reduction of the optimal design is 39.19 dB compared with the baseline beam

Concluding Remarks

This paper studied the multi-objective optimal design of non-uniform beams for minimum sound radiation. The structural weight and radiated sound power are two objective functions. The MOPSO algorithm is used to search for the optimal solutions. The transfer matrix method is used to obtain solutions of vibration and sound radiation of non-uniform beams with high efficiency and accuracy that are required in optimization studies. We discovered that when practical constraints such as the smoothness and lower bound of the fundamental frequency of the structure are imposed, the feasible solutions can be found in only a very small subset of the design space. Numerical results of multi-objective optimal design of non-uniform beams with two different boundary conditions are presented. We have shown that the optimized non-uniform beam has a smaller radiated sound power and radiation efficiency in the targeted frequency range compared with the uniform beam of the same mass.

Acknowledgements This work is supported by the National Natural Science Foundation of China (No. 51606180).

References

1. Au FTK, Zheng DY, Cheung YK (1999) Vibration and stability of non-uniform beams with abrupt changes of cross-section by using C1 modified beam vibration functions. Appl Math Model 23(1):19–34
2. Lee SY, Hsiao JY (2002) Free in-plane vibrations of curved nonuniform beams. Acta Mech 155(3–4):173–189
3. Purekar AS, Pines DJ (2000) Detecting damage in non-uniform beams using the dereverberated transfer function response. Smart Mater Struct 9(4):429–444
4. Chen LY, Wang DY (2007) Structural-acoustic optimization of stiffened panels based on a genetic algorithm. J Mar Sci Appl 6(4):55–61
5. Sun JQ (1995) Vibration and sound radiation of non-uniform beams. J Sound Vib 185(5):827–843
6. Ho SH, Chen CK (1998) Analysis of general elastically end restrained non-uniform beams using differential transform. Appl Math Model 22(4):219–234
7. Adali S (1983) Pareto optimal design of beams subjected to support motions. Comput Struct 16(1–4):297–303
8. Eschenauer H, Kneppe G, Stenvers K (1986) Deterministic and stochastic multiobjective optimization of beam and shell structures. J Mech Transm Autom Design 108(1):31–37
9. Kodiyalam S, Adali S, Sadek IS (1992) Multiobjective design optimization of continuous beams by numerical methods. Eng Comput 9(5):539–546
10. Denli H, Sun JQ (2008) Optimization of boundary supports for sound radiation reduction of vibrating structures. J Vib Acoust 130(1):011007
11. Joshi P, Mulani S, Kapania R (2011) Multi-objective vibro-acoustic optimization of stiffened panels excited by acoustic diffuse field. In: Proceedings of the 52nd AIAA/ASME/ASCE/AHS/ASC Structures, Structural Dynamics and Materials Conference. Denver, Colorado, USA
12. Fliege J, Svaiter BF (2000) Steepest descent methods for multi-criteria optimization. Math Methods Oper Res 51(3):479–494
13. Custódio AL, Madeira JFA, Vaz AIF et al (2011) Direct multi-search for multiobjective optimization. SIAM J Optim 21(3):1109–1140
14. Ringkamp M, Ober-Blöbaum S, Dellnitz M et al (2012) Handling high-dimensional problems with multi-objective continuation methods via successive approximation of the tangent space. Eng Optim 44(9):1117–1146
15. Dellnitz M, Schuetze O, Hestermeyer T (2005) Covering Pareto sets by multilevel subdivision techniques. J Optim Theory Appl 124(1):113–136
16. Hernández C, Naranjani Y, Sardahi Y et al (2013) Simple cell mapping method for multi-objective optimal feedback control design. Int J Dyn Control 1(3):231–238
17. Naranjani Y, Hernández C, Xiong FR et al (2013) A hybrid algorithm for the simple cell mapping method in multi-objective optimization. In: Proceedings of EVOLVE—A bridge between probability, set oriented numerics, and evolutionary computing. Leiden, The Netherland
18. Deb K, Pratap A, Agarwal S et al (2002) A fast and elitist multiobjective genetic algorithm: NSGA-II. IEEE Trans Evol Comput 6(2):182–197
19. Deb K (2001) Multi-objective optimization using evolutionary algorithms. Wiley, Hoboken
20. Coello CAC, Pulido GT, Lechuga MS (2004) Handling multiple objectives with particle swarm optimization. IEEE Trans Evol Comput 8(3):256–279
21. Amuso VJ, Enslin J (2007) The strength Pareto evolutionary algorithm 2 (SPEA2) applied to simultaneous multi-mission waveform design. In: Proceedings of the International Waveform Diversity and Design Conference 407–417
22. Coello CAC, Lechuga MS (2002) MOPSO: a proposal for multiple objective particle swarm optimization. Proc Congr Evol Comp 2:1051–1056
23. Poli R, Kennedy J, Blackwell T (2007) Particle swarm optimization. Swarm Intell 1(1):33–57
24. Coello CAC, Veldhuizen DAV, Lamont GB (2002) Evolutionary algorithms for solving multi-objective problems. Springer, Berlin